Materials Research Express

PAPER

The effect on electrical and luminescent properties in nanocrystalline $Na_{0.5}Bi_{0.5-x}Nd_xTiO_3$

To cite this article: G Thirupathi *et al* 2017 *Mater. Res. Express* **4** 095019

Materials Research Express

PAPER

The effect on electrical and luminescent properties in nanocrystalline $Na_{0.5}Bi_{0.5-x}Nd_xTiO_3$

RECEIVED
20 June 2017

REVISED
24 August 2017

ACCEPTED FOR PUBLICATION
25 August 2017

PUBLISHED
20 September 2017

G Thirupathi, Kumara Raja Kandula, Sai Santosh Kumar Raavi and Saket Asthana

Advanced Functional Materials Laboratory, Department of Physics, Indian Institute of Technology Hyderabad, Kandi (V), Sangareddy 502285, India

E-mail: asthanas@iith.ac.in and sskraavi@iith.ac.in

Keywords: hydrothermal synthesis, nanocrystalline, lead free piezoceramics, TEM studies, luminescence

Abstract

In this work, we report the simultaneous optimization of the relaxor properties and photoluminescence from nanocrystalline Nd^{3+} substituted NBT ($Na_{0.5}Bi_{0.5-x}Nd_xTiO_3$ where $x = 0, 0.01, 0.02$ and 0.04) synthesized by hydrothermal method. Substitution of optically active Nd^{3+} results in luminescence in addition to the modification of structural and electrical properties of the parent NBT. NBT-Nd ceramics stabilize in a rhombohedral structure which is confirmed by x-ray diffraction analysis. Here, the long-range structure is associated with the removal of local strain inhomogeneity by hydrothermal synthesis. The variation of morphology observed from the transmission electron micrographs is conjectured to be the result of the nucleation process involved with Nd^{3+} content in hydrothermal process. The Raman spectral measurements concur with the observed rhombohedral symmetry. Upon photo-excitation typical NIR emission from Nd^{3+} in the NIR region is observed. The variation in the dielectric and the optical properties correlate well with the structural observations for NBT-Nd compositions.

Introduction

Rare earth modified ferroelectric materials are useful in photonic and microelectronic devices like high-speed light modulators, oscillators and nonlinear frequency converters. The microscopic functionality in ferroelectrics i.e. transition temperature, dynamics of domain, dielectric and ferroelectric properties, and piezoelectric response can be modified at nanoscales [1, 2]. Recently, the synthesis and growth of different nanostructures (nanowires, particles, tubes etc) are explained by Varghese *et al*, for nanoferroelectric applications [3]. The optical activity in ferroelectric crystals is demonstrated as laser action and intracavity self-frequency conversion where their multi-functionality increases in integrated photonic devices. The NBT-host is chosen for rare earth doping because of its environmental-friendly ferroelectric and piezoelectric nature with high Curie temperature. The origin of the global monoclinic like structure of NBT is due to the structural and strain inhomogeneity present locally, instead of the existence of a thermodynamic equilibrium state [4–6]. According to Rao *et al* [7], this inhomogeneity can be controlled by electrical poling which in turn establishes the long range rhombohedral structure. Hydrothermal method is a low cost and green preparation technique used for crystallization. Here, the local strain inhomogeneity can be minimized to establish long range rhombohedral structure for the NBT without poling. The hydrothermal method allows us to control the crystal growth, nucleation process and homogeneity depending on the experimental conditions involved i.e. temperature, pressure, duration, mineralizer concentration and the ratio of the precursors. The process also provides the uniform structure (single phase) and morphological control due to the uniform temperature and pressure inside the autoclave which is more important in the synthesis of nanostructured materials [8, 9]. The electrical properties are quite different in the cases of nanosize when compared to bulk counterparts [10, 11]. It is quite challenging to study electrical properties at nanoscales due to experimental limitations and the involvement of the quantum phenomena [12]. Hence, the variation of electrical properties of NBT-Nd shows significant influence on the particle sizes. The ferroelectric host (NBT) is chosen to introduce the optical activity by the doping of Nd^{3+} ions. The electronic state of the ferroelectric NBT can be modified slightly with rare-earth substitution at the Bi-site due to structural parameters variations. Therefore, the effect of rare earth (Nd) modified NBT is associated with local structure

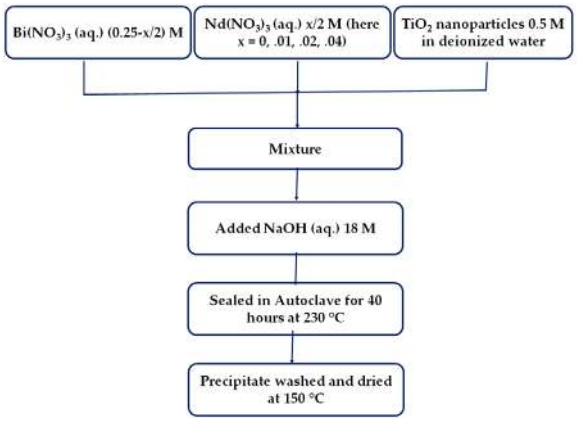

Figure 1. Schematic diagram of hydrothermal process.

Figure 2. CCD camera image of the pellets of the compositions Nd00, Nd01, Nd02 and Nd04 (left to right) under white light respectively.

which introduces considerable change in the electrical and optical properties of the NBT [13, 14]. The Nd^{3+} substitution provides optical absorption spectra in the visible range corresponding to the respective optical excitations [15]. The charge configuration and ionic size of Nd^{3+} prefer the substitution at the Bi-site of NBT in its stoichiometric conditions. The electrical and the optical properties of nano NBT-Nd have been investigated in detail to optimize the system for the fabrication of electro-optical devices.

Experimental details

The nanocrystalline $Na_{0.5}Bi_{0.5-x}Nd_xTiO_3$ (NBT-Nd, where $x = 0$, 0.01, 0.02 and 0.04) were synthesized via hydrothermal method and abbreviated as NBT, NBT-Nd01, NBT-Nd02 and NBT-Nd04 respectively. All the chemicals used are of high purity AR-grade (Sigma-Aldrich). The stoichiometric precursors, $Bi(NO_3)_3$, $Nd(NO_3)_3$ and TiO_2 nanoparticles, were taken in deionized water for the synthesis of NBT-Nd nano-compositions. The solution was added to 18 M of NaOH and after thorough stirring the resultant was immediately autoclaved at 230 °C for 40 h. The solution occupied 65% of the volume of the Teflon vessel in the autoclave. The hydrothermal procedure is followed as per the schematic diagram as shown in figure 1. Similar hydrothermal synthesis is reported for the NBT by other research groups [16–18]. The chemical equation is follows:

$$0.5\,Bi(NO_3)_3 + 1TiO_2 + n\text{NaOH} \rightarrow Na_{0.5}Bi_{0.5}TiO_3 + 1.5NaNO_3 + (n-2)\text{NaOH} + H_2O.$$

Here '*n*' depends on the concentration of the NaOH which is related to the ratio of OH^- ions to Ti^{3+} ions (18:0.5) and the volume of the deionized water (50 ml) used for the synthesis. The obtained powder was washed with deionized water several times to remove the excess NaOH and dried at 150 °C. The pellets were prepared with optimized load for electrical characterizations. Figure 2 shows the colour variation of NBT-Nd pellets captured using a CCD camera. The colour change also indicates the variation in optical properties at nanoscale.

The x-ray diffraction (XRD) pattern was recorded using an x-ray diffractometer (Panalytical X'pert Pro) equipped with Cu-K_α source in the range of 20°–80° with 0.5 ° min^{-i} scan speed to confirm the phase formation. The Rietveld refinements were performed using the Fullprof suite program for the XRD data. Raman spectral measurements were obtained using a Laser Micro Raman spectrometer (Bruker, Senterra) in a back-scattering geometry. The FEI Tecnai G2 S-Twin 200 kV transmission electron microscope (TEM) was used for the micro-structural studies. The obtained powder for the NBT-Nd samples were pelletized by the addition of polyvinyl alcohol (PVA) as a binder. The pellets were kept for binder evaporation at 600 °C for 4 h. The temperature dependent dielectric measurements were performed on the silver coated pellets from 30 to 450 °C along with the frequency variation between 20 Hz and 1 MHz using an impedance analyser (Wayne Kerr 6500B). The optical properties were investigated using diffusion reflectance spectra (LAMBDA 1050). The PL spectral measurements

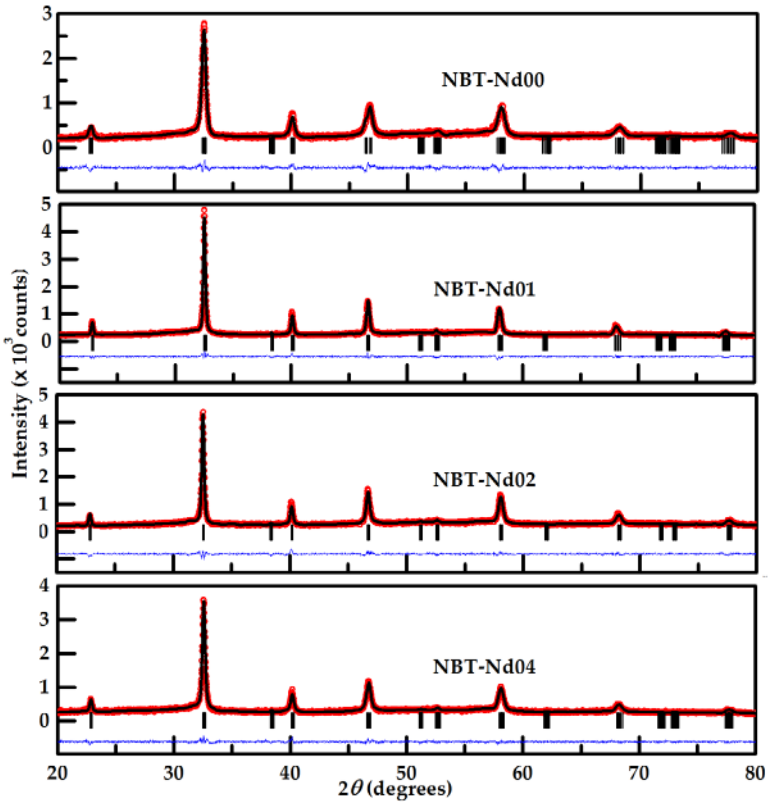

Figure 3. XRD pattern of NBT-Nd for Nd = 0, 0.01, 0.02 and 0.04 respectively.

were performed with a fiber-coupled spectrometer (AvaSpec-ULS2048L-RS, Avantes) by photo-exciting with 532 nm from a cw-DPSS laser (LSR532NL-300, Lasever).

Results and discussion

Figure 3 shows the XRD pattern of NBT-Nd (Nd = 0, 0.01, 0.02 and 0.04). The XRD patterns were well fitted with Rietveld refinement by considering rhombohedral (space group *R3c*) phase [19]. The refined patterns indicate the non-existence of global monoclinic structure due to the minimization of local strain homogeneities. It is worth mentioning that the *R3c* phase is stabilized without electrical poling throughout the hydrothermally synthesized compounds. The refined structural parameters are summarized in table 1. The average crystallite size (L) is found to increase with Nd^{3+} substitution, as estimated from the Williamson–Hall (WH) plot, indicating improved crystallinity. The broadness in the reflections indicates the formation of nanoscale NBT-Nd.

Figure 4 depicts the variation of lattice parameters with Nd-content in the NBT nano ceramics. The lattice parameters increase first for Nd = 0.01 from NBT and further values are decreasing for Nd = 0.02 and 0.04 and approaches the same value as for NBT. The peaks shift towards higher angle due to the substitution of Nd^{3+} ion (1.27 Å) at Bi^{3+} (1.37 Å) site which confirms the incorporation of Nd^{3+} ion at Bi-site. The variation in the lattice parameters including volume is not significant which could be due to the smaller concentration of substitution. This size variation can easily be accommodated within the generated lattice strain. Generally, the smaller ionic radii element creates internal chemical pressure which supports the disorderness at A-site. The structural studies confirm the incorporation of a smaller percentage of Nd- at Bi-site which is required for the optimization of optical properties without compromising the NBT properties. Therefore, the host environment with optimal Nd-content can be explored to tune the optical properties under the electric fields [20].

Figure 5 shows the Raman spectra of NBT-Nd compounds. The Raman modes are resolved into four regions according to the vibrational frequency range of different vibrations of the ions or bonds of the NBT. The lowest frequency modes (region-A) are dominated by the displacements of A-site cations (Bi-ions). These modes are observed to be well resolved here compared to the modes of NBT bulk [21, 22]. This means using the vibrational modes of Bi-site, the local structure influencing can be probed more in the nano range. There is no considerable change observed for the modes in region B and C compared to the bulk behaviour of NBT where the vibrations NaO and TiO_6 (octahedral) dominate, respectively [23]. Similarly, the modes in range D associated with Oxygen vibrations seem to be stable with the bulk comparison. Therefore, the Raman spectra of NBT indicates the Bi-site is more influenced by the hydrothermal nano preparation. The rapid decrease in the intensity and broadening of

Table 1. The structural parameters from XRD of NBT-Nd composites.

Composition	Nd00	Nd01	Nd02	Nd04
$a(=b)$ (Å)	5.496	5.505	5.498	5.492
c (Å)	13.474	13.492	13.479	13.468
V (Å^3)	352.4	354.1	352.9	351.9
Na, Bi, Nd (x, y, z)	0, 0, 0.25	0, 0, 0.25	0, 0, 0.25	0, 0, 0.25
Ti (x, y, z)	0, 0, 0.010	0, 0, 0.008	0, 0, 0.011	0, 0, 0.0099
O (x, y, z)	0.17, 0.38, 0.06	0.17, 0.37, 0.06	0.17, 0.37, 0.06	0.15, 0.36, 0.06

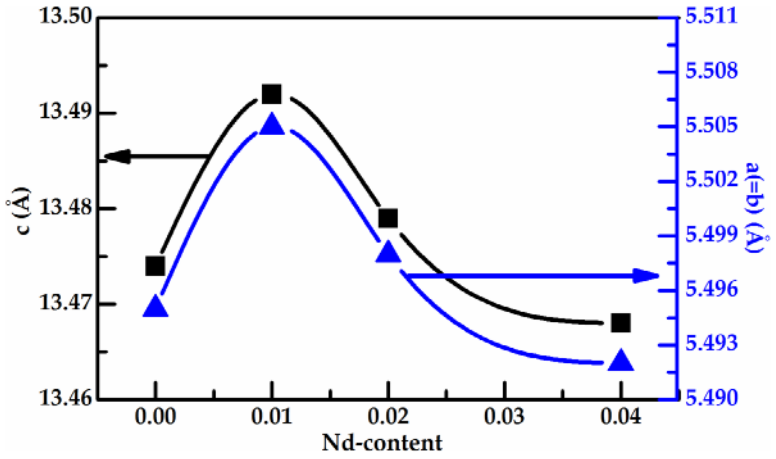

Figure 4. Lattice parameters as function of Nd-content in NBT.

modes and the shift of A-band towards a lower wavenumber confirm the incorporation of Nd- at Bi-site [24, 26]. Apart from the A-site disorder, the relatively broadened phonon bands can be attributed to the variation of local structure of NBT without changing the long-range symmetry [25, 27]. In other words, the broad nature of the Raman bands is due to the substitutional disorder at A-site [28, 29].

Figure 6 depicts the TEM micrographs of NBT nanowires and nano-NBT-Nd04 and electron diffraction pattern of NBT-Nd04. The formation of the nanowires is due to the nucleation process involved in the NBT as Na–Ti–O seed for the growth of one dimensional nanostructures. The nucleation transforms to cubes and grows homogeneously into nanocrystals with Nd-substitution. The typical micrograph for higher Nd-content NBT is shown in figure 4(d). A similar cubic shaped pattern has been observed in NBT-Nd01 and NBT-Nd02. The crystal planes in the electron diffraction pattern are also indexed with *R*3*c* indices which is consistent with observations from XRD and Raman studies (typical pattern for NBT-Nd04 is shown in figure 4(c)). This indicates the growth process is enhanced to form nanocrystals (cuboid) for the Nd-substitutions [30]. It has been noticed that the morphology depends on the hydrothermal parameters as well as the compositions. The small Nd-content addition transforms the nanowires (NBT) to the cuboid structure.

The different morphologies (including the crystal structure, size and shape of the particles) are the function of temperature, pressure, time, concentration and compositions used in the hydrothermal process. The changes in the morphology may also be caused by the lattice expansion resulted from the Nd-substitution using hydrothermal synthesis The nucleation process is affected by the substitution of Nd-in NBT and transformed to cuboid [31]. The nanostructures are observed to be uniform with narrow size distribution due to the nucleation process which was controlled with uniform hydrothermal pressure and temperature accommodated in the sealed Teflon vessel.

Figure 7 depicts the AC conductivity of NBT-Nd compositions at various temperatures. The frequency dependent conductivity spectra follow the Jonscher power law: $\sigma_{ac}(\omega) = \sigma_{dc} + A\omega^{S}$. The spectra converged to the low conductivity value at low frequencies due to the space charge polarization which creates greater opposition to the flow of charge carriers in NBT-Nd nano-ceramics. In the case of polycrystalline materials, the a.c conductivity depends on charge carrier density, the grain size and the scattering at the grain boundaries. Further, the conductivity should be increased when the NBT is modified by the carrier element. On the contrary, here the decreasing trend in conductivity is observed with Nd-content. Even though the electronic bands shift to improve conductivity, the crystal structure plays a major role in the conduction mechanism where the local disorders are prominent with the substitutions as compared to the parent NBT compound. Figure 8 shows the Arrhenius plots of the nano NBT and NBT-Nd compositions for the conductivity. The activation energy (E_a) varies from 1.1 to

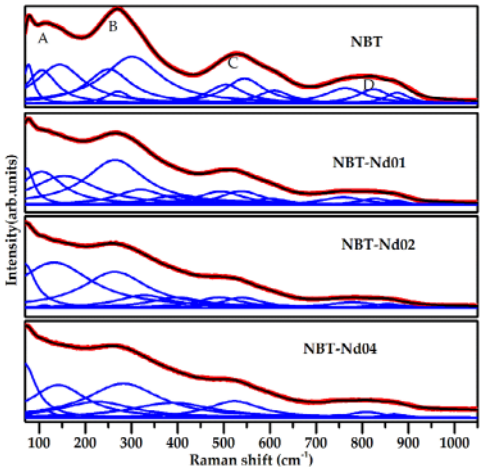

Figure 5. Raman spectra of NBT-Nd for Nd = 0, 0.01, 0.02 and 0.04 respectively.

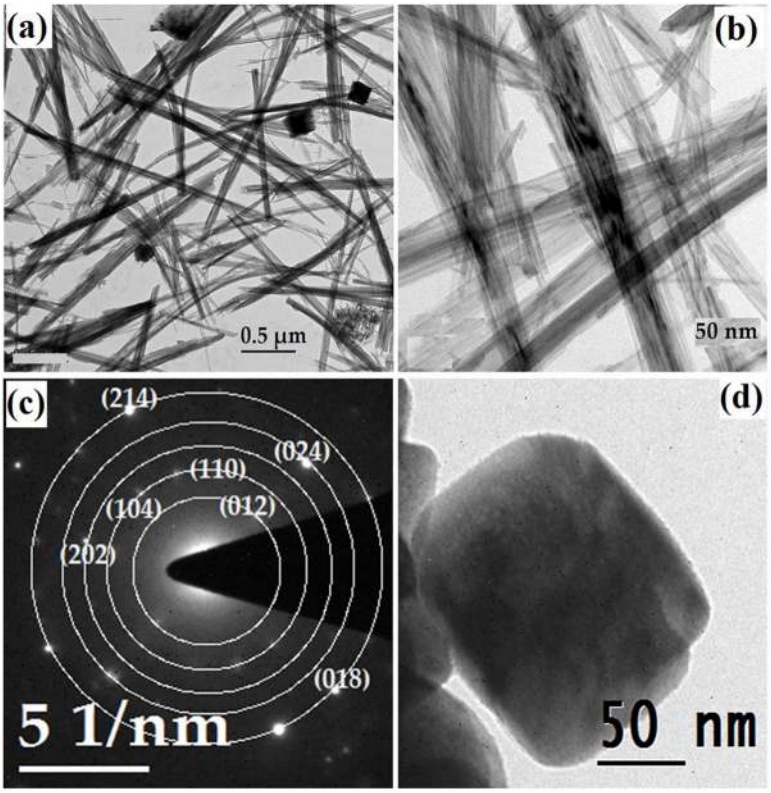

Figure 6. TEM micrographs of NBT nanowires (a) and (b) and electron diffraction pattern and TEM micrograph of NBT-Nd04 (c) and (d) respectively.

1.5 eV for the Nd00, and Nd04 compounds. The observation of a high activation energy is related to the reduction of oxygen vacancies contributing to the conduction and the separation of charge cluster characteristic for the compositions [32, 33]. From figure 8, the order of DC conductivity of Nd00 and Nd04 differs from that of Nd01 and Nd02 compositions which could be due to the inhomogeneous distribution of vacancies which modifies the conduction mechanism.

The dielectric properties of nano Nd-NBT are useful in finding optimized conditions for enhanced relaxor systems with synthesis and composition. The variation of dielectric constant with frequency shows a similar trend but it differs in the order of dielectric constant which makes sense in understanding the influence of structural changes. The dielectric constant is enhanced for Nd01 and it is suppressed for Nd02 and Nd04 compositions. This is due to the modification of local structure or crystal environment with Nd-content in NBT. The off-centered position of Bi^{3+} and the A-site occupation by Na^{+} and Bi^{3+} ions create the inhomogeneous local electric and strain fields which refers to the degree of cationic disorder. The relaxor-like features can be modified by the A-site disorders in NBT. Figure 9 shows the temperature dependent dielectric plots of NBT-Nd at various

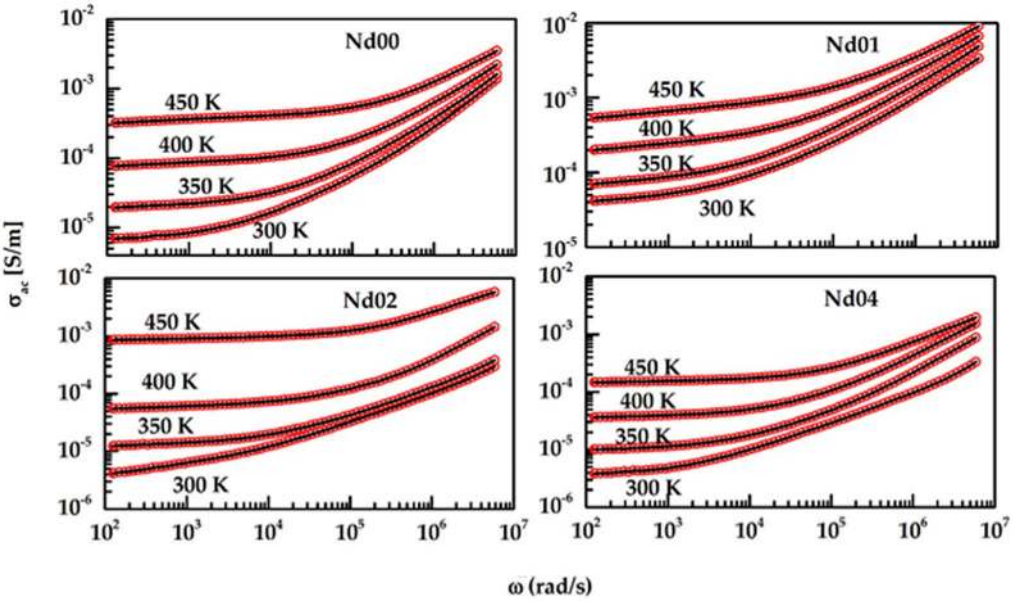

Figure 7. Conductivity as a function of frequency at various temperatures.

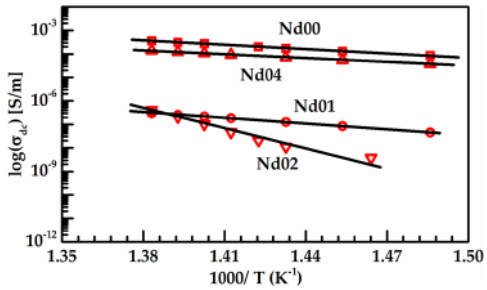

Figure 8. Arrhenius plots and the activation energy as function of Nd-content.

frequencies. Initially, the dielectric constant is high due to the nano-ferroelectric clusters at room temperature. And it decreases sharply when the temperature is increased. Recently, similar relaxor results have been presented with the grain size effect by Tan *et al* [34]. Moreover, the ferroelectric order could not sustain long range order due to nanosize where the maximum ferroelectric domain is limited by the nanocrystal size. Therefore, the ferroelectric to antiferroelectric transition (T_d) cannot be differentiated in the plots. However, the paraelectric transition temperature which is usually accompanied by a dielectric maximum (T_m) is observed in the plots. The radius and polarizability of guest ions (Nd^{3+}) differs from that of Na^{+} and Bi^{3+}. It can be inferred that the incorporation of the Nd^{3+} ions at Bi-site will change the degree of cationic disorder and this may enhance the relaxor-like features in NBT-Nd. The *Tm*-value is 275 °C for Nd00 and Nd04 and the value is 325 °C for Nd01 and Nd02. The Nd01 compound showed broad and high Curie transition. This indicates the relaxor-like behaviour is optimum for Nd01 among the compositions which is supported by the structural changes from the XRD results.

Figure 10 depicts the UV–visible absorption spectra of nano NBT-Nd compositions. The optical bandgap (E_g) is obtained experimentally from the extrapolation of absorption edge in the Tauc's region. Here $h\nu$ or hc/λ is the photon energy. The E_g-values are ~3.16 eV for samples Nd00, Nd02 and Nd03 whereas the value is 3.13 eV for the Nd01 sample [25]. The change in E_g-value (red shift) is related to the structural variation where the lattice expansion is observed by the introduction of 1% Nd in the NBT-host. The inset figure is a magnified view of the UV absorption spectra where the optical excitations are expected. Similar UV absorption results are reported for Nd-NBT by Zannen *et al* [35]. The peaks observed are related to the optical excitation for the existing transitions for Nd ions [36–38]. In pure NBT, there is no absorption observed relating to the optical excitation. So, the radiative transitions take place when the NBT is doped with Nd^{3+} ions.

Figure 11 shows the PL spectra of nano NBT-Nd compositions. The Nd^{3+} ions are excited by green laser of the wavelength (λ_{exc}) of 532 nm and the luminescence is observed in the frequency range of 13 000–9000 cm^{-1} (750–1100 nm). The NBT is optically inactive and the emissions are observed when the host lattice is introduced by the emitter ions (Nd^{3+}) at Bi-site. These emissions are attributed to the optical radiation band transitions in Nd^{3+}

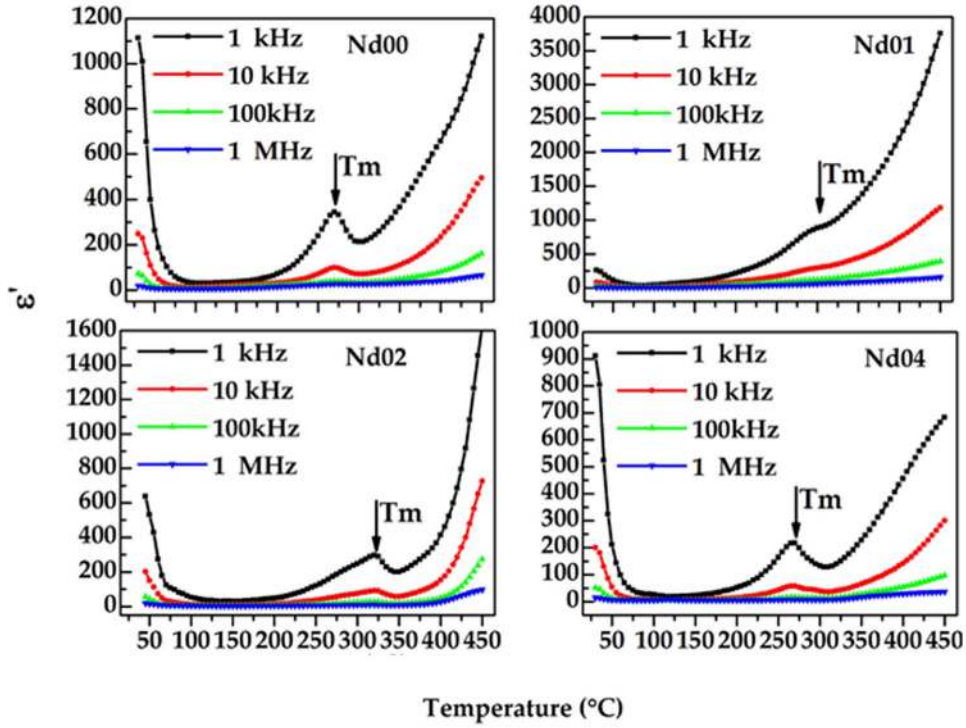

Figure 9. The temperature dependent dielectric curves of NBT-Nd at various frequencies.

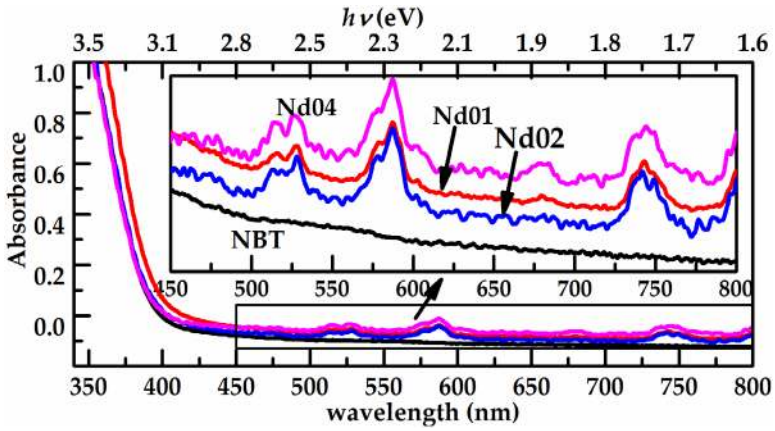

Figure 10. The UV–visible diffuse reflectance spectra (inset is zoomed view of the absorbance for the corresponding excitations) of nano NBT-Nd compositions.

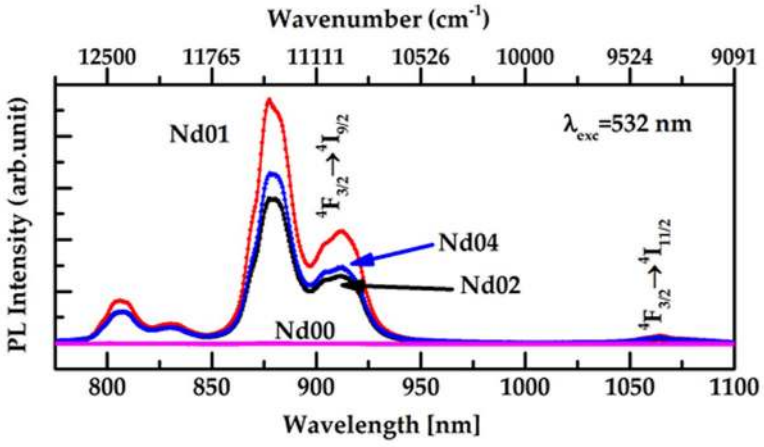

Figure 11. The PL spectra of nano NBT-Nd compositions.

ions from $^4F_{3/2} \rightarrow {}^4I_{9/2}$ and $^4F_{3/2} \rightarrow {}^4I_{11/2}$ in the vicinity of the wavelengths 880 nm and 1060 nm respectively [39]. The similar optical transitions are shown in the Nd-NBT by He *et al* with λ_{exc} of 808 nm [40]. However, the highest PL intensity is observed for the Nd01 composition. The change in the environment of relaxor ferroelectric systems will differ in crystal field strengths giving rise to slight changes in the PL intensity [20, 41]. Here, the lattice expansion for Nd01 (from XRD results) is due to the sharing of Nd^{3+} ions by surrounding unit cells of the Bi-site to stabilize in the homogeneous structure. When the Nd-content is increased, the sufficient number of Nd^{3+} ions will be available where the system tries to retain the NBT structure. So, the local crystal structure of the NBT is more disturbed when the Nd-content is very small. And due to the lattice void in the expanded crystal structure, it is easy to probe the PL of the optically excited Nd^{3+} ions where the PL intensity will be obtained maximum. It is clear that the optimized Nd-content should be less than 1% for obtaining high PL.

Conclusions

The synthesis using the hydrothermal route and characterization of nanocrystalline Nd^{3+} substituted NBT has been reported. The effect of nanostructured ceramics on the structural electrical and optical properties have been explored. The formation of nano-ceramics has been confirmed through TEM studies. The rhombohedral phase *R3c* is stabilized in nano-NBT and Nd-substituted NBT without electrical poling which cannot be observed in bulk NBT. The variation in the electrical properties have been observed with the substitution and explained in terms of size effect. The best PL intensity has been observed in the 1% Nd-substituted NBT. The effect of nanosize on functional properties seems to be promising to explore in other lead free systems.

Acknowledgment

RSSK acknowledges the financial support from DST (YSS/2015/000008) and CSIR [03(1348)16/EMR-II]. SA acknowledges DST Project No.EMR/2014/000761 for financial support.

ORCID iDs

Sai Santosh Kumar Raavi https://orcid.org/0000-0002-2496-9233
Saket Asthana https://orcid.org/0000-0002-6420-3304

References

[1] Nan C-W, Bichurin M I, Dong S, Viehland D and Srinivasan G 2008 *J. Appl. Phys.* **103** 31101
[2] Boutinaud P, Cavalli E, Velchuri R and Vithal M 2012 *J. Phys.: Condens. Matter* **24** 75502
[3] Varghese J, Whatmore R W and Holmes J D 2013 *J. Mater. Chem.* C **1** 2618
[4] Thangavelu K and Asthana S 2015 *Mater. Res. Express* **2** 96301
[5] Guennou M, Savinov M, Drahokoupil J, Luo H and Hlinka J 2013 *Appl. Phys.* A **116** 225
[6] Hiruma Y, Nagata H and Takenaka T 2009 *J. Appl. Phys.* **105** 84112
[7] Rao B N, Datta R, Chandrashekaran S S, Mishra D K, Sathe V, Senyshyn A and Ranjan R 2013 *Phys. Rev.* B **88** 224103
[8] Hou Y-D, Hou L, Zhao J-L, Zhu M-K and Yan H 2011 *J. Electroceramics* **26** 37
[9] Iqbal A, Iqbal Y, Chang L, Ahmed S, Tang Z and Gao Y 2012 *J. Nanopart. Res.* **14** 1206
[10] Zhou Y, Yang M, Sun K, Tang Z and Kotov N A 2010 *J. Am. Chem. Soc.* **132** 6006
[11] Sahu M, Karthik T, Srinivas A and Asthana S 2015 *J. Mater. Sci. Mater. Electron.* **26** 9741
[12] Cain M G (ed) 2014 *Characterisation of Ferroelectric Bulk Materials and Thin Films* (Dordrecht: Springer)
[13] Qin B, Chen H, Liang H, Fu L, Liu X, Qiu X, Liu S, Song R and Tang Z 2010 *J. Am. Chem. Soc.* **132** 2886
[14] Castillejo M, Ossi P M and Zhigilei L (ed) 2014 *Lasers in Materials Science* (Cham: Springer International Publishing)
[15] Yune J H, Karatchevtseva I, Triani G, Wagner K and Officer D 2013 *J. Mater. Res.* **28** 488
[16] Zhou X, Jiang C, Chen C, Luo H, Zhou K and Zhang D 2016 *CrystEngComm* **18** 1302
[17] Li B, Cao M-S, Liu J and Wang D-W 2016 *J. Am. Ceram. Soc.* **99** 2316
[18] Zhang H, Liu L, Zhu M, Hou Y, Wang R and Yan H 2016 *Int. J. Appl. Ceram. Technol.* **13** 569
[19] Kumari R, Ahlawat N, Agarwal A, Sanghi S, Sindhu M and Ahlawat N 2016 *J. Magn. Magn. Mater.* **414** 1
[20] Khatua D K, Kalaskar A and Ranjan R 2016 *Phys. Rev. Lett.* **116** 117601
[21] Niranjan M K, Karthik T, Asthana S, Pan J and Waghmare U V 2013 *J. Appl. Phys.* **113** 194106
[22] Barick B K, Mishra K K, Arora A K, Choudhary R N P and Pradhan D K 2011 *J. Phys. Appl. Phys.* **44** 355402
[23] Huang T, Guo S, Xu L P, Chen C, Hu Z G, Luo H S and Chu J H 2015 *J. Appl. Phys.* **117** 224103
[24] Suchanicz J, Bovtun V, Dutkiewicz E M, Konieczny K, Sitko D, Kluczewska K, Wajda A, Kalvane A and Sternberg A 2016 *Phase Transit.* **89** 856
[25] Huang T, Hu Z G, Xu G S, Zhang X L, Zhang J Z and Chu J H 2014 *Appl. Phys. Lett.* **104** 111908
[26] Roukos R J, Bidault O, Pansiot J, Minier L and Saviot L 2011 *Adv. Mater. Res.* **324** 298
[27] Zannen M, Khemakhem H, Kabadou A and Es-Souni M 2013 *J. Alloys Compd.* **555** 56
[28] Tripathy S N, Mishra K K, Sen S and Pradhan D K 2014 *J. Am. Ceram. Soc.* **97** 1846
[29] Chen Y, Lam K H, Zhou D, Dai J Y, Luo H S, Jiang X P and Chan H L W 2013 *Integr. Ferroelectr.* **141** 120
[30] Han J-M, Joung M-R, Kim J-S, Lee Y-S, Nahm S, Choi Y-K and Paik J-H 2014 *J. Am. Ceram. Soc.* **97** 346
[31] Sun Y, Liu H, Hao H, Song Z and Zhang S 2015 *J. Am. Ceram. Soc.* **98** 1574

[32] Malathi A R, Kumar G S and Prasad G 2015 *Phase Transit.* **88** 169
[33] Kao K C 2004 *Dielectric Phenomena in Solids: with Emphasis on Physical Concepts of Electronic Processes* (Amsterdam: Elsevier)
[34] Tan Y, Zhang J, Wu Y, Wang C, Koval V, Shi B, Ye H, McKinnon R, Viola G and Yan H 2015 *Sci. Rep.* **5** 9953
[35] Zannen M, Lahmar A, Dietze M, Khemakhem H, Kabadou A and Es-Souni M 2012 *Mater. Chem. Phys.* **134** 829
[36] Shanmugavelu B, Venkatramu V and Ravi Kanth Kumar V V 2014 *Spectrochim. Acta* A **122** 422
[37] Lenz C, Nasdala L, Talla D, Hauzenberger C, Seitz R and Kolitsch U 2015 *Chem. Geol.* **415** 1
[38] Tobaldi D M, Ferreira R A S, Pullar R C, Seabra M P, Carlos L D and Labrincha J A 2015 *J. Mater. Chem.* C **3** 4970
[39] Elleuch R, Salhi R, Deschanvres J-L and Maalej R 2014 *Chem. Phys. Lett.* **612** 1
[40] He C, Zhang Y, Sun L, Wang J, Wu T, Xu F, Du C, Zhu K and Liu Y 2013 *J. Phys. Appl. Phys.* **46** 245104
[41] Miao F J, Tao B R, Jiang K, Zhang J Z, Li W W, Hu Z G, Chu J H and Chu P K 2013 *J. Phys. Appl. Phys.* **46** 315105